J|A|C|S
ARTICLES
Published on Web 04/05/2006

Nanoscale Patterning of Two Metals on Silicon Surfaces Using an ABC Triblock Copolymer Template

Masato Aizawa* and Jillian M. Buriak*

Contribution from the National Institute for Nanotechnology and the Department of Chemistry, University of Alberta, Edmonton, Alberta, Canada T6G 2G2

Received January 17, 2006; E-mail: maizawa@ualberta.ca; jburiak@ualberta.ca

Abstract: Patterning technologically important semiconductor interfaces with nanoscale metal films is important for applications such as metallic interconnects and sensing applications. Self-assembling block copolymer templates are utilized to pattern an aqueous metal reduction reaction, galvanic displacement, on silicon surfaces. Utilization of a triblock copolymer monolayer film, polystyrene-*block*-poly(2-vinylpyridine)-*block*-poly(ethylene oxide) (PS-*b*-P2VP-*b*-PEO), with two blocks capable of selective transport of different metal complexes to the surface (PEO and P2VP), allows for chemical discrimination and nanoscale patterning. Different regions of the self-assembled structure discriminate between metal complexes at the silicon surface, at which time they undergo the spontaneous reaction at the interface. Gold deposition from gold(III) compounds such as $HAuCl_4$(aq) in the presence of hydrofluoric acid mirrors the parent block copolymer core structure, whereas silver deposition from Ag(I) salts such as $AgNO_3$(aq) does the opposite, localizing exclusively under the corona. By carrying out gold deposition first and silver second, sub-100-nm gold features surrounded by silver films can be produced. The chemical selectivity was extended to other metals, including copper, palladium, and platinum. The interfaces were characterized by a variety of methods, including scanning electron microscopy, scanning Auger microscopy, X-ray photoelectron spectroscopy, and atomic force microscopy.

Introduction

Metallization of semiconductors with micrometer-scale and nanoscale control plays an important role in the production of integrated devices. Controlling size, shape, and locations of metallic nanoparticles on semiconductors in periodic arrangements is considered to be a key for future nanoelectronic applications.[1] Scanning probe tip-mediated approaches such as dip-pen nanolithography (DPN)[2] and other direct writing methods like electron beam lithography[3] are powerful tools to define metallic nanoscale features on surfaces, among others. In terms of highly parallel synthetic strategies, nanofabrication techniques using self-assembled nanostructures are particularly attractive due to their efficiency and high-throughput.[4] Block copolymer templates represent an exciting group of self-assembled structures because of their compatibility with existing silicon-based fabrication techniques,[5] commercial availability, and incredible diversity of chemistries and morphologies.[6−8] Since block copolymers contain two or more chemically differentiated polymer chains, they demonstrate selective solubilization of various chemical reagents; for instance, a polar block will sequester polar solutes, a block with metal donor ligands will selectively bind metal ions, etc. Block copolymers on surfaces can therefore be used to direct chemical reagents to an interface, at which they will undergo reactions that mirror the pattern of the polymer template.

Block copolymers containing a metal-binding block such as poly(4-vinylpyridine) (P4VP), in addition to a polystyrene block, are well established to form self-assembled hexagonal arrays

(1) (a) Mieszawska, A. J.; Zamborini, F. P. *Chem. Mater.* **2005**, *17*, 3415. (b) Lin, H. H.; Gao, T.; Fantini, J.; Sailor, M. J. *Langmuir* **2005**, *21*, 1661. (c) Zamborini, F. P.; Smart, L. E.; Leopold, M. C.; Murray, R. W. *Anal. Chim. Acta* **2003**, *496*, 3. (d) Huang, J. X.; Kim, F.; Tao, A. R.; Connor, S.; Yang, P. D. *Nature Mater.* **2005**, *4*, 896. (e) Plaza, J. L.; Mendes, P. M.; Diegoli, S.; Chen, Y.; Preece, J. A.; Palmer, R. E. *J. Nanosci. Nanotechnol.* **2005**, *5*, 1826. (f) Shenhar, R.; Jeoung, E.; Srivistava, S.; Norsten, T. B.; Rotello, V. M. *Adv. Mater.* **2005**, *17*, 2206. (g) Park, J. I.; Lee, W. R.; Bae, S. S.; Kim, Y. J.; Yoo, K. H.; Cheon, J.; Kim, S. *J. Phys. Chem. B* **2005**, *109*, 13119. (h) Foster, E. W.; Kearns, G. J.; Goto, S.; Hutchinson, J. E. *Adv. Mater.* **2005**, *17*, 1542. (i) McMillan, R. A.; Howard, J.; Zaluzec, N. J.; Kagawa, H. K.; Mogul, R.; Li, Y.-F.; Paavola, C. D.; Trent, J. D. *J. Am. Chem. Soc.* **2005**, *127*, 2800. (j) Wong, E. W.; Bronikowski, M. J.; Hoenk, M. E.; Kowalczyk, R. S.; Hunt, B. D. *Chem. Mater.* **2005**, *17*, 237. (k) Su, P. Y.; Hu, J. C.; Cheng, S. L.; Chen, L. J.; Liang, J. M. *Appl. Phys. Lett.* **2004**, *84*, 3480.

(2) (a) Ginger, D. S.; Zhang, H.; Mirkin, C. A. *Angew. Chem., Int. Ed.* **2004**, *43*, 30. (b) Hong, S.; Mirkin, C. A. *Science* **2000**, *288*, 1808. (c) Piner, R. D.; Zhu, J.; Xu, F.; Hong, S.; Mirkin, C. A. *Science* **1999**, *283*, 661. (d) Li, Y.; Maynor, B. W.; Liu, J. *J. Am. Chem. Soc.* **2001**, *123*, 2105. (e) Porter, J. L., Jr.; Choi, H. C.; Schmeltzer, J. M.; Ribble, A. E.; Elliott, L. C. C.; Buriak, J. M. *Nano Lett.* **2002**, *2*, 1369. (f) Su, M.; Dravid, V. P. *Appl. Phys. Lett.* **2002**, *80*, 4434. (g) Nyamjav, D.; Ivanisevic, A. *Adv. Mater.* **2003**, *15*, 1805.

(3) (a) Craighead, H. G. *Science* **2000**, *290*, 1532. (b) Ito, T.; Okazaki, S. *Nature* **2000**, *406*, 1027. (c) Pashkin, Y.; Nakamura, Y.; Tsai, J. S. *Appl. Phys. Lett.* **2000**, *76*, 2256. (d) Liu, K.; Avouris, P.; Bucchignano, J.; Martel, R.; Sun, S.; Michl, J. *Appl. Phys. Lett.* **2002**, *80*, 865.

(4) (a) Allred, D. B.; Sarikaya, M.; Baneyx, F.; Schwartz, D. T. *Nano Lett.* **2005**, *5*, 609. (b) Hawker, C. J.; Russell, T. P. *MRS Bull.* **2005**, *30*, 952. (c) Ryu, D. Y.; Shin, K.; Drockenmuller, E.; Hawker, C. J.; Russell, T. P. *Science* **2005**, *308*, 236. (d) Marrian, C. R. K.; Tennant, D. M. *J. Vac. Sci. Technol. A* **2003**, *21*, S207. (e) Khomutov, G. B.; Kislov, V. V.; Antipina, M. N.; Gainutdinov, R. V.; Gubin, S. P.; Obydenov, A. Y.; Pavlov, S. A.; Rakhnyanskaya, A. A.; Sergeev-Cherenkov, A. N.; Soldatov, E. S.; Suyatin, D. B.; Tolstikhina, A. L.; Trifonov, A. S.; Yurova, T. V. *Microelectron. Eng.* **2003**, *69*, 373.

(5) (a) Black, C. T.; Bezencenet, O. *IEEE Trans. Nanotechnol.* **2004**, *3*, 412. (b) Guarini, K. W.; Black, C. T.; Zhang, Y.; Kim, H.; Sikorski, E. M.; Babich, I. V. *J. Vac. Sci. Technol. B* **2002**, *20*, 2788.

of P4VP micelles on solid surfaces when spin- or dip-coated from a nonpolar solvent like toluene.[9−11] The nitrogen of the pyridine units in the P4VP block coordinates to, or is protonated by, metal ions and compounds such as auric acid ($HAuCl_4$).[7,11] We have demonstrated that this block copolymer template may be used for spatial direction of surface chemistry exclusively via the P4VP block of the template. $HAuCl_4$ and Ag^+ ions coordinated within the hydrophilic P4VP block of monolayers of self-assembled PS−P4VP block copolymers on semiconductor interfaces such as silicon, germanium, gallium arsenide, and indium phosphide are reactive toward surface chemistry.[12] Through a galvanic displacement reaction, the gold and silver ions were spontaneously reduced to metallic Au and Ag by these materials, resulting in bound, patterned metal nanoparticles whose size and average separation were dictated by the parent block copolymer. This technique allows one to produce monometallic, pseudo-hexagonal arrays of Au or Ag nanoparticles on the surfaces with precise control over particle size and interparticle distance.

More challenging is the preparation of interfaces with two, or perhaps more, different nanoscale metal features, also with nanoscale spatial and size control. In order to direct two different chemical reagents sequentially to the surface in a manner analogous to positive and negative masking, judicious choice of selective polymer blocks is required. The ability of chemically differentiated blocks of a block copolymer to selectively solubilize chemical reagents is becoming established. Previous work by several groups has demonstrated sequestration of metal complexes and other materials, such as metal nanoparticles, within diverse blocks.[8,13−16] For instance, anionic complexes such as $AuCl_4^-$, $PtCl_4^{2-}$, and $PdCl_4^{2-}$ interact selectively with the protonated P2VP block of poly(2 (or 4)-vinylpyridine)-*block*-poly(ethylene oxide) diblock copolymers (P2VP-*b*-PEO) at pH < 5,[13] while with the poly(butadiene)-*block*-poly(ethylene oxide) polymer (PB-*b*-PEO), complexes such as $(CH_3CN)_2PdCl_2$ and $KPt(C_2H_4)Cl_3$ interact with the double bonds of PB via π-complexes.[14] To the best of our knowledge, there has been only one report involving block copolymer templating of two metal nanostructures within the block copolymer. Sohn, Teranishi, and co-workers solubilized $FeCl_3$ in the core of PS−P4VP, and dodecanethiol-terminated Au nanoparticles in the PS portion; upon oxygen plasma treatment, γ-Fe_2O_3 nanoparticles formed in the core, surrounded by a corona of Au nanoparticles on a transmission electron microscopy grid.[10] This growing body of literature suggests that the ability of block copolymers to direct chemical reagents to a surface is a viable approach to surface patterning since they are obviously selective with respect to incorporation of various chemical reagents.

In this paper, we describe nanoscale patterning of two kinds of metals on silicon using a self-assembled monolayer of triblock copolymers, polystyrene-*block*-poly(2-vinylpyridine)-*block*-poly(ethylene oxide) (PS-*b*-P2VP-*b*-PEO), as a template. Transition metal complexes are delivered to different nanoscale areas of the surface utilizing the intrinsic selectivity of the P2VP and PEO blocks toward various metal ions, and then they undergo spontaneous reduction via galvanic displacement with silicon. Gold chloride anions (derived from $HAuCl_4$, $KAuCl_4$, and $AuCl_3$ precursors)[17] are selectively coordinated in the P2VP block and are reduced to metallic Au nanoparticles underneath the block copolymer core/shell, while Ag^+ ions, on the other hand,

(6) (a) Antonietti, M.; Wenz, E.; Bronstein, L.; Seregina, M. *Adv. Mater.* **1995**, *7*, 1000. (b) Antonietti, M.; Foerster, S.; Hartmann, J.; Oestreich, S. *Macromolecules* **1996**, *29*, 3800. (c) Hillmyer, M. A.; Lipic, P. M.; Hajduk, D. A.; Almdal, K.; Bates, F. S. *J. Am. Chem. Soc.* **1997**, *119*, 2749. (d) Webber, S. E. *J. Phys. Chem. B* **1998**, *102*, 2618. (e) Cox, J. K.; Eisenberg, A.; Lennox, R. B. *Curr. Opin. Colloid Interface Sci.* **1999**, *4*, 52. (f) Spontak, R. J.; Alexandridis, P. *Curr. Opin. Colloid Interface Sci.* **1999**, *4*, 140. (g) Zehner, R. W.; Sita, L. R. *Langmuir* **1999**, *15*, 6139. (h) Hahm, J.; Sibener, S. J. *Langmuir* **2000**, *16*, 4766. (i) Thurn-Albrecht, T.; Steiner, R.; DeRouchey, J.; Stafford, C. M.; Huang, E.; Bal, M.; Tuominen, M.; Hawker, C. J.; Russell, T. P. *Adv. Mater.* **2000**, *12*, 787. (j) Thurn-Albrecht, T.; Schotter, J.; Kastle, G. A.; Emley, N.; Shibauchi, T.; Krusin-Elbaum, L.; Guarini, K.; Black, C. T.; Tuominen, M. T.; Russell, T. P. *Science* **2000**, *290*, 2126. (k) Boeker, A.; Mueller, A. H. E.; Krausch, G. *Macromolecules* **2001**, *34*, 7477. (l) Haupt, M.; Miller, S.; Bitzer, K.; Thonke, K.; Sauer, R.; Spatz, J. P.; Mossmer, S.; Hartmann, C.; Moller, M. *Phys. Status Solidi B* **2001**, *224*, 867. (m) Krausch, G.; Magerle, R. *Adv. Mater.* **2002**, *14*, 1579. (n) Liu, T.; Burger, C.; Chu, B. *Prog. Polym. Sci.* **2002**, *28*, 5. (o) Meli, M.-V.; Badia, A.; Gruetter, P.; Lennox, R. B. *Nano Lett.* **2002**, *2*, 131. (p) Balsara, N. P.; Hahn, H. *Chem. Nanostruct. Mater.* **2003**, 317. (q) Cuenya, B. R.; Baeck, S.-H.; Jaramillo, T. F.; McFarland, E. W. *J. Am. Chem. Soc.* **2003**, *125*, 12928. (r) Jaramillo, T. F.; Baeck, S.-H.; Cuenya, B. R.; McFarland, E. W. *J. Am. Chem. Soc.* **2003**, *125*, 7148. (s) Foerster, S. *Top. Curr. Chem.* **2003**, 226, 1. (t) Hamley, I. W. *Nanotechnology* **2003**, *14*, R39. (u) Hamley, I. W. *Angew. Chem., Int. Ed.* **2003**, *42*, 1692. (v) Jaramillo, T. F.; Baeck, S.-H.; Cuenya, B. R.; McFarland, E. W. *J. Am. Chem. Soc.* **2003**, *125*, 7148. (w) Lazzari, M.; Lopez-Quintela, M. A. *Adv. Mater.* **2003**, *15*, 1583. (x) Liu, G. *Polym. Prepr. (Am. Chem. Soc., Div. Polym. Chem.)* **2003**, *44*, 208. (y) Park, C.; Yoon, J.; Thomas, E. L. *Polymer* **2003**, *44*, 6725. (z) Raez, J.; Tomba, J. P.; Manners, I.; Winnik, M. A. *J. Am. Chem. Soc.* **2003**, *125*, 9546. (aa) Cheng, J. Y.; Jung, W.; Ross, C. A. *Phys. Rev. B* **2004**, *70*, 064417. (bb) Hamley, I. W. Introduction to Block Copolymers. In *Developments in Block Copolymer Science and Technology*; Hamley, I. W., Ed.; John Wiley & Sons: West Sussex, England, 2004; p 1. (cc) Ikkala, O.; ten Brinke, G. *Chem. Commun.* **2004**, 2131. (dd) Sundrani, D.; Darling, S. B.; Sibener, S. J. *Langmuir* **2004**, *20*, 5091. (ee) Filali, M.; Meier, M. A. R.; Schubert, U. S.; Gohy, J.-F. *Langmuir* **2005**, *21*, 7995. (ff) Lin, Y.; Boeker, A.; He, J.; Sill, K.; Xiang, H.; Abetz, C.; Li, X.; Wang, J.; Emrick, T.; Long, S.; Wang, Q.; Balazs, A.; Russell, T. P. *Nature* **2005**, *434*, 55. (gg) Wan, J.; Alizadeh, A.; Taylor, S. T.; Malenfant, P. R. L.; Manoharan, M.; Loureiro, S. M. *Chem. Mater.* **2005**, *17*, 5613. (hh) Segalman, R. *Mater. Sci. Eng. R* **2005**, *48*, 191.

(7) Glass, R.; Moeller, M.; Spatz, J. P. *Nanotechnology* **2003**, *14*, 1153.

(8) Sakai, T.; Alexandridis, P. *Nanotechnology* **2005**, *16*, 344.

(9) (a) Hahn, J.; Webber, S. E. *Langmuir* **2004**, *20*, 4211. (b) Meli, M.-V.; Badia, A.; Grutter, P.; Lennox, R. B. *Nano Lett.* **2002**, *2*, 131. (c) Sohn, B.; Yoo, S.; Seo, B.; Yun, S.; Park, S. *J. Am. Chem. Soc.* **2001**, *123*, 12734. (d) Spatz, J. P. *Angew. Chem., Int. Ed.* **2002**, *41*, 3359. (e) Spatz, J. P.; Eibeck, P.; Moessmer, S.; Moeller, M.; Kramarenko, E. Y.; Khalatur, P. G.; Potemkin, I. I.; Khokhlov, A. R.; Winkler, R. G.; Reineker, P. *Macromolecules* **2000**, *33*, 150. (f) Spatz, J. P.; Herzog, T.; Moessmer, S.; Ziemann, P.; Moeller, M. *Adv. Mater.* **1999**, *11*, 149. (g) Spatz, J. P.; Moessmer, S.; Hartmann, C.; Moeller, M.; Herzog, T.; Krieger, M.; Boyen, H.-G.; Ziemann, P.; Kabius, B. *Langmuir* **2000**, *16*, 407. (h) Spatz, J. P.; Moller, M.; Ziemann, P. *Phys. Bl.* **1999**, *55*, 49. (i) Spatz, J. P.; Roescher, A.; Sheiko, S.; Krausch, G.; Moeller, M. *Adv. Mater.* **1995**, *7*, 731.

(10) Sohn, B.; Choi, J.; Yoo, S.; Yun, S.; Zin, W.; Jung, J.; Kanehara, M.; Hirata, T.; Teranishi, T. *J. Am. Chem. Soc.* **2003**, *125*, 6368.

(11) (a) Spatz, J. P.; Chan, V. Z. H.; Mossmer, S.; Kamm, F.-M.; Plettl, A.; Ziemann, P.; Moller, M. *Adv. Mater.* **2002**, *14*, 1827. (b) Spatz, J. P.; Sheiko, S.; Moeller, M. *Macromolecules* **1996**, *29*, 3220.

(12) Aizawa, M.; Buriak, J. M. *J. Am. Chem. Soc.* **2005**, *127*, 8932.

(13) (a) Vamvakaki, M.; Papoutsakis, L.; Katsamanis, V.; Afchoudia, T.; Fragouli, P. G.; Iatrou, H.; Hadjichristidis, N.; Armes, S. P.; Sidorov, S.; Zhirov, D.; Zhirov, V.; Kostylev, M.; Bronstein, L. M.; Anastasiadis, S. H. *Faraday Discuss.* **2004**, *128*, 129. (b) Semagina, N. V.; Bykov, A. V.; Sulman, E. M.; Matveeva, V. G.; Sidorov, S. N.; Dubrovina, L. V.; Valetsky, P. M.; Kiselyova, O. I.; Khokhlov, A. R.; Stein, B.; Bronstein, L. M. *J. Mol. Catal. A: Chem.* **2004**, *208*, 273. (c) Bronstein, L. M.; Sidorov, S. N.; Valetshy, P. M.; Hartmann, J.; Colfen, H.; Antonietti, M. *Langmuir* **1999**, *15*, 6256. (d) Bronstein, L. M.; Sidorov, S. N.; Zhirov, V.; Zhirov, D.; Kabachii, Y. A.; Kochev, S. Y.; Valetsky, P. M.; Stein, B.; Kiseleva, O. I.; Polyakov, S. N.; Shtykova, E. V.; Nikulina, E. V.; Svergun, D. I.; Khokhlov, A. R. *J. Phys. Chem. B* **2005**, *109*, 18786. (e) Sidorov, S. N.; Bronstein, L. M.; Kabachii, Y. A.; Valetshy, P. M.; Soo, P. L.; Maysinger, D.; Eisenberg, A. *Langmuir* **2004**, *20*, 3543.

(14) Bronstein, L.; Kramer, E.; Berton, B.; C, B.; Forster, S.; Antonietti, M. *Chem. Mater.* **1999**, *11*, 1402.

(15) (a) Sidorov, S. N.; Bronstein, L. M.; Valetshy, P. M.; Hartmann, J.; Colfen, H.; Schnablegger, H.; Antonietti, M. *J. Colloid Interface Sci.* **1999**, *212*, 197. (b) Bronstein, L. M.; Sidorov, S. N.; Gourkova, A. Y.; Valetshy, P. M.; Hartmann, J.; Breulmann, M.; Colfen, H.; Antonietti, M. *Inorg. Chim. Acta* **1998**, *280*, 348. (c) Filali, M.; Meier, M. A. R.; Schubert, U. S.; Gohy, J.-F. *Langmuir* **2005**, *21*, 7995.

(16) (a) Zhang, D.; Qi, L.; Ma, J.; Cheng, H. *Chem. Mater.* **2001**, *13*, 2753. (b) Wang, L.; Chen, X.; Zhao, J.; Sui, Z.; Zhuang, W.; Xu, L.; Yang, C. *Colloids Surf. A* **2005**, *257*, 231.

(17) $AuCl_3$ in an HX acid will form AuX_4^- anions. Cotton, F. A.; Willkinson, G.; Murillo, C. A.; Bochman, M. *Advanced Inorganic Chemistry*, 6th ed.; John Wiley & Sons: New York, 1999; p 1101.

undergo reduction exclusively in the PEO corona. It was possible to form Au−core and Ag−corona nanostructures on the surface by subsequently depositing Au and Ag. Among other metals examined, Na_2PdCl_4 and Na_2PtCl_4 are coordinated and reduced under the P2VP block, while Cu^{2+} is reduced to nanoparticles under the PEO block.

Experimental Section

Generalities. Unless otherwise noted, all the experiments were performed under ambient conditions. Si(100) (p-type, B-doped, $\rho = 0.01-0.02\ \Omega\cdot$cm) wafers were purchased from Addison Engineering. $KAuCl_4\cdot xH_2O$, $AuCl_3$ (99%), $AgNO_3$ (99.99995%), $AgClO_4\cdot H_2O$ (99%), $AgCH_3COO$ (99%), AgF (98%), $Na_2PtCl_4\cdot xH_2O$, $Na_2PdCl_4\cdot 3H_2O$ (99%), and $CuSO_4\cdot 5H_2O$ (99.999%) were purchased from Strem Chemicals, whereas $HAuCl_4$ (99.9995%) was purchased from Sigma-Aldrich. The ABC triblock copolymer, polystyrene-*block*-poly(2-vinylpyridine)-*block*-poly(ethylene oxide) (PS-*b*-P2VP-*b*-PEO, with molecular weights of 20 000, 14 000, and 26 000 for the PS, P2VP, and PEO blocks, respectively), was purchased from Polymer Source (www.polymersource.com). Water was obtained from a Millipore system (resistivity >18 MΩ). *N*,*N*-Dimethylformamide (DMF), benzene, and toluene used in this study were HPLC grade (Sigma-Aldrich), and the methanol was Optima grade (Fisher). HF(aq) (49%), H_2O_2(aq) (30%), HCl(aq) (36.5−38.0%), and NH_4OH(aq) (10−35%) were semiconductor grade, obtained from J. T. Baker. NH_4F (40%) was purchased as a solution from Riedel-deHaen. All reagents listed above were used without further purification. Teflon beakers and tweezers were used exclusively during the cleaning and preparation of the Si wafers and for all metal deposition procedures.

Surface Characterization. Metal nanostructures on silicon were characterized by atomic force microscopy (AFM), scanning electron microscopy (SEM), scanning Auger microcopy (SAM), and X-ray photoelectron spectroscopy (XPS). SEM, SAM, and XPS were performed under high-vacuum conditions ($<10^{-8}$ Torr). The atomic force microscope used in this study was a Nanoscope IV (Digital Instruments/Veeco) using commercially available Si cantilevers in tapping mode under ambient conditions. SEM (Hitachi S-4800 FE-SEM) of metal nanostructures was typically performed with an electron energy of 10 keV, while a reduced electron energy (5 keV) was employed in order to image polymer-coated silicon surfaces to minimize damage. SAM (JEOL, JAMP-9500F) was carried out with an electron accelerating voltage and emission current of 25 kV and 6 nA, respectively. The Auger peaks of Si KL23L23 (1600 eV), Ag M4N45N45 (350 eV), and Au M5N67N67 (2015 eV) were selected for the mapping. The Auger mapping for each element was obtained by plotting $(P - B)/B$, where P and B are peak and background intensities, respectively. The intensities were then scaled using the JEOL processing software for increased contrast. The average escape depths for Au and Ag MNN electrons from SiO_2 are estimated to be ∼4.2 and ∼1.1 nm, respectively, according to the NIST IMFP database.[18] XPS (Kratos Analytical, Axis-Ultra) was performed using monochromatic Al Kα with a photon energy of 1486.6 eV. The average escape depths for Au 4f and Ag 3d electrons from SiO_2 are estimated to be ∼3.2 and ∼2.6 nm, respectively, according to the NIST IMFP database. The instrument was calibrated on the basis of the C 1s. The Ag 3d and Au 4f metallic positions were also calibrated using sputtered Ag and Au films, respectively.

Silicon Cleaning Procedures. Pieces of Si(100) measuring ∼7 mm^2 were degreased in a methanol ultrasonic bath for 15 min and dried with a nitrogen stream. The wafers were then cleaned via standard RCA cleaning procedures.[19] The wafers were first immersed in a hot solution of H_2O:NH_4OH:H_2O_2 (5:1:1) for 15 min. After the wafers were rinsed with excess water, they were immersed in another hot solution of H_2O:HCl:H_2O_2 (6:1:1) for 15 min. The wafers were again rinsed with an excess amount of water. Following this cleaning procedure, the wafers were visibly hydrophilic; water on the surface was immediately removed with a stream of nitrogen before polymer spin-coating.

Polymer Template Preparation. Core−shell−corona micelles were prepared in pure water from the triblock copolymers using the method developed by Jerôme and co-workers.[20] Briefly, ∼2 wt % polymer solutions were prepared by dissolving PS-*b*-P2VP-*b*-PEO in a 0.9 g mixture of DMF and benzene, ensuring that the proportion of DMF was kept to 70−75 wt %. A 0.1 mL volume of water was then added to the solution under vigorous stirring in order to initiate the polymer self-assembly, and stirring was maintained for at least 12 h. After the micelles were kinetically frozen with 1 mL of water, the organic solvent mixture was dialyzed against water for 5 days to recover the micelles in pure water. The typical polymer solution used for spin-coating was diluted to ∼0.5 wt %.

Single-Metal Galvanic Displacement Deposition on Silicon. A piece of cleaned Si(100) was spin-coated (Laurell, WS-400B-6NPP-Lite) using 10 μL of the diluted polymer solution at 5000 rpm for 1 min. The polymer-coated wafer was then immersed in a mixture of 1 mL of 1 mM aqueous metal salt and 9 mL of 1% HF(aq) for a given time [final solution concentration is therefore 0.1 mM aqueous metal salt/0.9% HF(aq)]. ***WARNING:*** *Hydrofluoric acid (HF) is extremely hazardous in both the liquid (aqueous) and vapor forms and can cause severe tissue damage upon contact with skin or via respiration.* After metal deposition, the sample was thoroughly rinsed with water and dried under a nitrogen stream. For Au and Ag deposition, the polymer templates were dissolved in a toluene ultrasound bath (Cole Palmer, 08891-021) for 5 min, and the sample was dried under a nitrogen stream. For the Cu, Pd, and Pt deposition, however, an H_2/Ar plasma (Harrick Plasma, PDC 32G, 18 W) was employed to remove the polymers since removal by toluene ultrasonication led to dissociation of the metal nanoparticles from the surface.

Au/Ag Mixed Structure Galvanic Displacement on Silicon. Two separate reaction vessels were used to sequentially pattern Au and Ag nanoparticles on silicon. First, a polymer-coated silicon shard was immersed in a mixture of 1 mL of 1 mM $HAuCl_4$(aq) and 9 mL of 1% HF(aq) [final solution concentration is therefore 0.1 mM $HAuCl_4$(aq)/0.9% HF(aq)] and rinsed with copious water to avoid further gold deposition on the surface. The sample was then immersed in the second vessel containing 1 mL of 1 mM $AgNO_3$(aq) and 9 mL of 1% HF(aq) [final solution concentration is therefore 0.1 mM $AgNO_3$(aq)/0.9% HF(aq)]. The sample was again rinsed with excess water and the polymer removed in a toluene ultrasound bath for 5 min, followed by drying under a nitrogen stream.

Electroless Deposition Growth of Au Nanoparticles on Silicon. The continuous Au nanostructures on silicon (Figure 3e,f) were obtained on the basis of the seed-mediated, electroless deposition method developed by Zamborini and co-workers.[1a,21] First, Au nanoparticles with diameters <10 nm were prepared by immersing a polymer-coated silicon shard into a mixture of 1 mL of 1 mM $HAuCl_4$(aq) and 9 mL of 1% HF(aq) for 1 min [final solution concentration is therefore 0.1 mM $HAuCl_4$(aq)/0.9% HF(aq)]. The sample was subsequently immersed into the electroless growth solution consisting of 9 mL of 0.1 M cetyltrimethylammonium bromide (CTAB), 450 μL of 0.01 M $HAuCl_4$(aq), and 0.05 mL of 0.1 M ascorbic acid (AA). In this mixture, the CTAB and AA are shape-directing and weak reducing agents, respectively. The polymers were removed via a toluene ultrasound bath for 5 min, followed by drying under a nitrogen stream.

(18) Powell, C. J.; Jablonski, A. *NIST Electron Inelastic-Mean-Free-Path Database*, Version 1.1.; National Institute of Standards and Technology: Gaithersburg, MD, 2000.

(19) Kern, W. Overview and Evolution of Semiconductor Wafer Contamination and Cleaning Technology. In *Handbook of Semiconductor Wafer Cleaning Technology*; Kern, W., Ed.; Noyes Publications: Park Ridge, NJ, 1993; p 3.

(20) (a) Lei, L.; Gohy, J.-F.; Willet, N.; Zhang, J.-X.; Varshney, S.; Jerôme, R. *Macromolecules* **2004**, *37*, 1089. (b) Lei, L.; Gohy, J.-F.; Willet, N.; Zhang, J.-X.; Varshney, S.; Jerôme, R. *Polymer* **2004**, *45*, 4375.

(21) (a) Wei, Z.; Mieszawska, A. J.; Zamborini, F. P. *Langmuir* **2004**, *20*, 4322. (b) Wei, Z.; Zamborini, F. P. *Langmuir* **2004**, *20*, 11301. (c) Gao, J.; Bender, C. M.; Murphy, C. J. *Langmuir* **2003**, *19*, 9065.

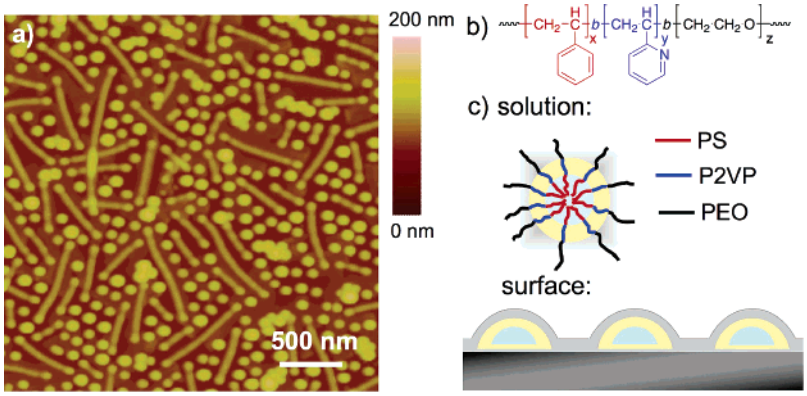

Figure 1. (a) AFM image of a monolayer of PS-*b*-P2VP-*b*-PEO triblock copolymers spin-coated onto a native oxide-capped Si(100) wafer. (b) Molecular structure of PS-*b*-P2VP-*b*-PEO. (c) Schematic structures of core−shell−corona micelles of the triblock copolymers in water and on a surface.

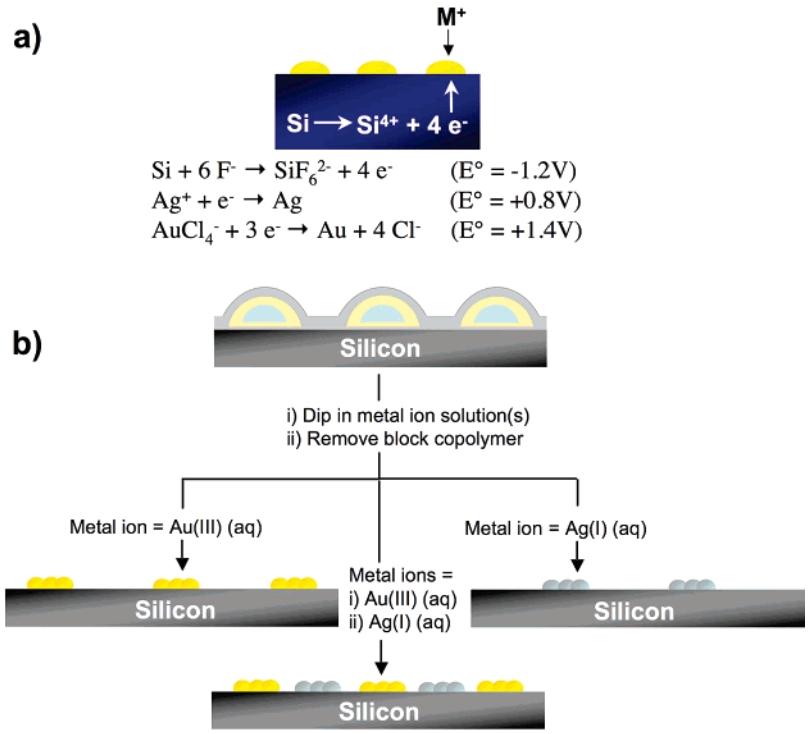

Figure 2. (a) Illustrative representation of galvanic displacement on silicon in the presence of hydrofluoric acid. The standard cell potentials shown are with respect to the normal hydrogen electrode (NHE). (b) Schematic representation of nanoscale patterning of Au and Ag on a silicon surface using the triblock copolymer as a template.

Results and Discussion

An ABC triblock copolymer containing three distinct chemical functionalities, polystyrene-*block*-poly(2-vinylpyridine)-*block*-poly(ethylene oxide) (PS-*b*-P2VP-*b*-PEO, with molecular weights of 20 000, 14 000, and 26 000 for the PS, P2VP, and PEO blocks, respectively), was chosen as the template. This polymer self-assembles into a mixture of rod-shaped and spherical micelles, each with a PS core and a P2VP shell, surrounded by a PEO corona.[20,22] Figure 1 shows an AFM image of a monolayer of self-assembled spherical and cylindrical micelles spin-coated onto a native oxide-capped silicon wafer, as well as their proposed structure, as shown in Figure 1c.[20] The diameter of the micelles is approximately 80 nm, and the cylindrical micelles are a few hundred nanometers to a micrometer in length. These polymer micelles were prepared as described in the Experimental Section, in a DMF/benzene solution with dropwise addition of a small amount of water, followed by kinetically freezing the micelles in water.[20] The as-formed micelles were recovered in pure water using dialysis and then spin-coated onto a native oxide-capped silicon wafer at 5000 rpm for 1 min. In order to bring about metal deposition via galvanic displacement, the polymer-coated silicon shard was immersed into an aqueous solution of the metal ion, in the presence of dilute hydrofluoric acid, at room temperature for the desired time (30 s to 1 h). The reduction process for these transition metal ions is best described by mixed potential theory, roughly based upon the half-cell reactions shown in Figure 2a; the silicon acts as a reducing agent and is oxidized to form silicon oxides that are dissolved by the dilute HF, enabling the

(22) (a) Gohy, J.-F.; Willet, N.; Varshney, S. K.; Zhang, J.-X.; Jerôme, R. *e-Polymer* **2002**, Paper No. 35. (b) Gohy, J.-F.; Willet, N.; Varshney, S.; Zhang, J.-X.; Jerôme, R. *Angew. Chem., Int. Ed.* **2001**, *40*, 3214. (c) Khanal, A.; Li, Y.; Takisawa, N.; Oishi, Y.; Nakashima, K. *Langmuir* **2004**, *20*, 4809. (d) Li, Y.; Khanal, A.; Kawasaki, N.; Oishi, Y.; Nakashima, K. *Bull. Chem. Soc. Jpn.* **2005**, *78*, 529.

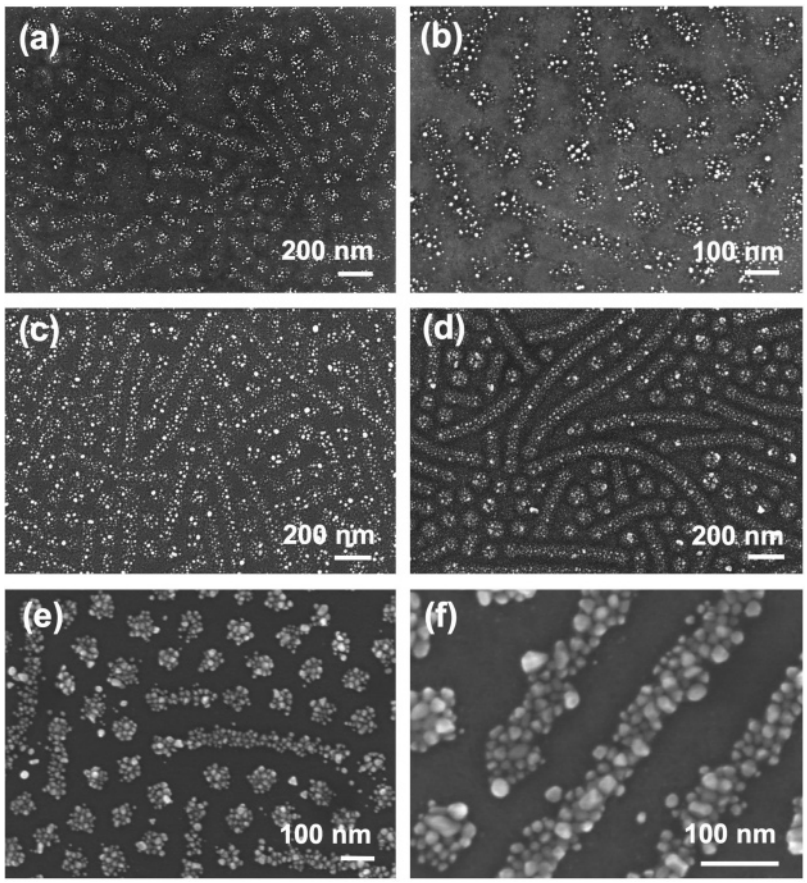

Figure 3. SEM images of Au nanostructures on SiO_x using the triblock copolymer as a template. The depositions were carried out from (a,b) 0.1 mM $KAuCl_4$/0.9% HF(aq) for 5 min, (c) 0.1 mM $HAuCl_4$/0.9% HF(aq) for 5 min, (d) 0.1 mM $AuCl_3$/0.9% HF(aq) for 5 min, (e) two-step deposition, involving 0.1 mM $HAuCl_4$/0.9% HF(aq) galvanic displacement for 1 min and then electroless deposition with 0.095 M $HAuCl_4$/4.7 $\times$ 10^{-4} M CTAB/5.3 $\times$ 10^{-4} M aqueous ascorbic acid for 60 min, and (f) the same conditions as (e) but the electroless deposition was carried out for 100 min.

reaction to continue.[23] Following removal of the silicon from the aqueous metal bath, the polymer was removed via dissolution in a toluene ultrasound bath for 5 min at room temperature.

Figure 3a−d shows SEM images of gold deposited on SiO_x-capped Si wafers using the PS-*b*-P2VP-*b*-PEO triblock as a template on silicon, from an aqueous gold(III) precursor solution ($KAuCl_4$, $HAuCl_4$, or $AuCl_3$),[17] in the presence of HF. Deposition of the gold nanoparticles closely follows the pattern of the PS/P2VP micelle rods and spheres, pointing to interaction of the AuX_4^- anion with the P2VP block; no significant deposition occurs underneath the PEO corona. This behavior is similar to previous results obtained using PS−P4VP templates on silicon as a result of the directing ability of the vinylpyridine block.[12]

Beyond 10 min of deposition time under these conditions, the gold nanoparticles have a tendency to be removed with the block copolymer due to the weak Si−Au interaction, most likely due to silicon etching that undercuts the deposited metal, releasing it with the polymer.[23c,24] Little difference was noted between $KAuCl_4$ and $HAuCl_4$ deposition under these conditions, although the fidelity of the $AuCl_3$ precursor with respect to the parent P2VP block is not as good as that of $KAuCl_4$/$HAuCl_4$, since some small-particle deposition between these blocks can be observed. Other anionic compound ions, such as $PdCl_4^{2-}$ and $PtCl_4^{2-}$, also deposit spontaneously in a similar manner, mirroring the spatial pattern of the gold precursors (Supporting Information). The P2VP block is expected to be protonated by hydrofluoric acid (the pK_a of a similar 2-substituted pyridine, protonated 2-methylpyridine, is 5.97, while the pK_a of HF is 3.17), meaning that the anionic metal complexes act as counteranions to the pyridinium group; the nature of their binding to the P2VP block is therefore electrostatic.[22a,b] The calculated pH of an aqueous solution with 1% HF(aq) is 1.7.

More continuous films of larger gold nanoparticles are produced if the $HAuCl_4$/HF(aq) is supplemented with an electroless reducing agent solution of ascorbic acid (AA) and the surfactant CTAB, as shown in Figure 3e,f.[1a,21] The surface is seeded with small gold nanoparticles produced via galvanic

(23) (a) Jones, D. A. *Principles and Prevention of Corrosion*; Macmillan: New York, 1992. (b) Okinaka, Y.; Osaka, T. *Adv. Electrochem. Sci. Eng.* **1994**, *3*, 55. (c) Magagnin, L.; Maboudian, R.; Carraro, C. *J. Phys. Chem. B* **2002**, *106*, 401. (d) Chemla, M.; Homma, T.; Bertagna, V.; Erre, R.; Kubo, N.; Osaka, T. *J. Electroanal. Chem.* **2003**, *559*, 111. (e) Peng, K.; Zhu, J. *Electrochim. Acta* **2004**, *49*, 2563. (f) Nagahara, L. A.; Ohmori, T.; Hashimoto, K.; Fujishima, A. *J. Vac. Sci. Technol. A* **1993**, *11*, 763. (g) Oskam, G.; Long, J. G.; Natarajan, A.; Searson, P. C. *J. Phys. D: Appl. Phys.* **1998**, *31*, 1927. (h) Niwa, D.; Homma, T.; Osaka, T. *J. Phys. Chem. B* **2004**, *108*, 9900. (i) Niwa, D.; Homma, T.; Osaka, T. *J. Phys. Chem. B* **2004**, *108*, 9900. (j) Lin, H.; Mock, J.; Smith, D.; Gao, T.; Sailor, M. J. *J. Phys. Chem. B* **2004**, *108*, 11654. (k) Porter, L. A.; Choi, H. C.; Buriak, J. M. *Nano Lett.* **2002**, *2*, 1067. (l) Zambelli, T.; Munford, M. L.; Pillier, F.; Bernard, M.-C.; Allongue, P. *J. Electrochem. Soc.* **2001**, *148*, C614. (m) Harraz, F. A.; Tsuboi, T.; Sasano, J.; Sakka, T.; Ogata, Y. H. *J. Electrochem. Soc.* **2002**, *149*, C456. (n) Sun, X.-H.; Wong, N.-B.; Li, C.-P.; Lee, S.-T.; Kim, P.-S. G.; Sham, T.-K. *Chem. Mater.* **2004**, *16*, 1143. (o) Takano, N.; Niwa, D.; Yamada, T.; Osaka, T. *Electrochim. Acta* **2000**, *45*, 3263. (p) Kim, C.; Oikawa, Y.; Shin, J.; Ozaki, H. *Microelectron. J.* **2003**, *34*, 607. (q) Gorostiza, P.; Allongue, P.; Díaz, R.; Morante, J. R.; Sanz, F. *J. Phys. Chem. B* **2003**, *107*, 6454.

(24) Nezhad, M. R. H.; Aizawa, M.; Porter, L. A., Jr.; Ribbe, A. E.; Buriak, J. M. *Small* **2005**, *1*, 1076.

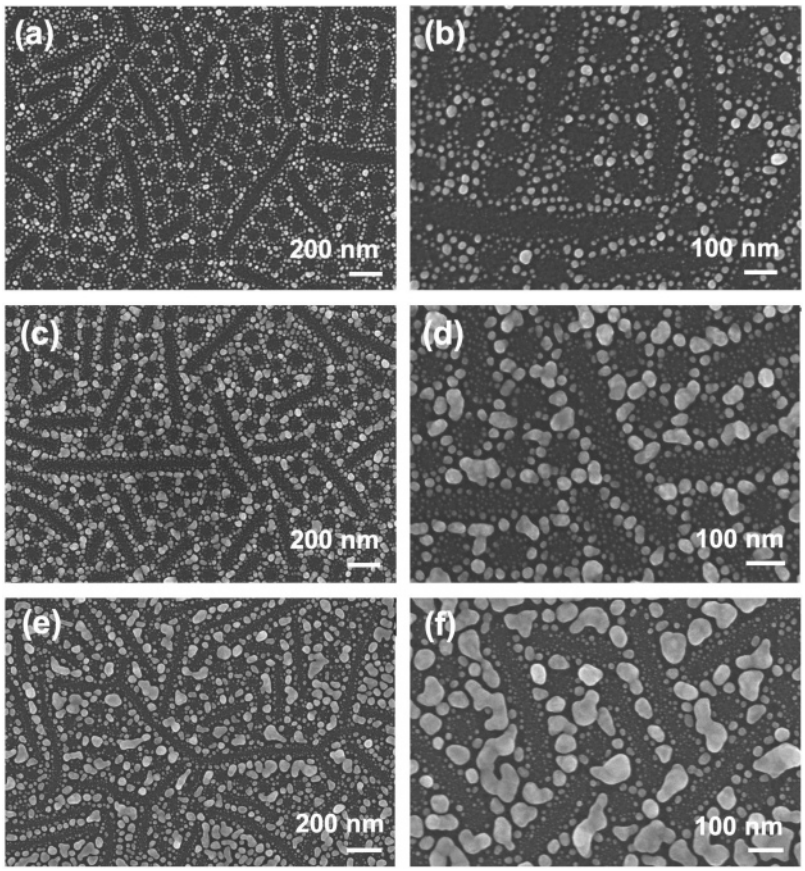

Figure 4. SEM images of Ag nanostructures on SiO_x using the triblock copolymer as a template, using a solution prepared from 0.1 mM $AgNO_3$/0.9% HF(aq), varying the time: (a,b) 5 min, (c,d) 20 min, (e) 40 min, and (f) 60 min.

displacement [1 min deposition in 0.1 mM $HAuCl_4$/0.9% HF-(aq)], followed by immersion in the AA/CTAB deposition bath for 60 min (Figure 3e) and 100 min (Figure 3f). The polymers were removed by a toluene ultrasound bath for 5 min. Further increases in the deposition time led to the larger quantities of Au deposition in both the PVP shell and the PEO corona. Because the initial galvanic displacement is carried out for only a short period of time, the films adhere well to the silicon surface, as subsequent growth is not reliant upon a mechanism that involves silicon corrosion and undercutting. The cationic surfactant protects the surface from nonselective deposition under these conditions, most likely via coordination to the silicon oxide that has a net negative charge.[25]

Silver nitrate deposition, as opposed to gold, results in silver deposition under the PEO corona, instead of the P2VP/PS blocks, leading to the opposite pattern, as shown in Figure 4. The Ag nanoparticles are larger toward the center of the PEO corona, up to approximately 30 nm in diameter, and are surrounded by smaller (<10 nm) silver nanoparticles, for deposition times of up to 10 min. At longer times (Figure 4c−f), silver particles up to 100 nm are formed. Other silver salts such as silver perchlorate and silver acetate, in the presence of fluoride, produce identical patterns (Supporting Information). Use of the water-soluble AgF salt, containing a fluoride counteranion, was tested to determine if the use of HF(aq) could be avoided, but this silver salt led to little observed deposition. Replacement of HF(aq) with 1% NH_4F(aq) was also unsuccessful for selective metal deposition, probably due to the aggressive nature of this etchant.

In terms of other metal salts that mirror the selectivity of Ag^+, copper(II) sulfate was tested since both are water-solvated cations, $[Ag(H_2O)_4]^+$ and $[Cu(H_2O)_6]^{2+}$ under these conditions.[26] Copper deposition also follows the PEO block of the parent polymer template (Supporting Information), but the weak Si−Cu interaction required block copolymer removal with H_2/Ar plasma since toluene ultrasonication resulted only in a pitted surface with no adhering copper metal. XPS of the copper(II) sulfate deposition before plasma treatment confirms that the metal is reduced via galvanic displacement since all the copper appears as Cu(0) (Supporting Information).

SAM was utilized to obtain compositional maps of a surface by forming an image from Auger electrons emitted by the elements of interest. Figures 5 and 6 are comprised of four images for each metal, gold and silver, prepared from $HAuCl_4$ and $AgNO_3$ precursors, in the presence of HF: (a) the SEM image taken with the scanning Auger microscope, (b) the elemental map for silicon (KLL signals), (c) the elemental map for the metal (MNN signals for Au or Ag), and (d) the combined silicon/metal elemental map (KLL/MNN). As can be seen from Figures 5e and 6e, the signals for Au/Ag and Si are opposite: the deposited metal masks the underlying silicon substrate, whereas in regions where the silicon is exposed, the signal for the metal is low. The scanning Auger images support the

(25) Chen, Z.; Singh, R. K. *J. Electrochem. Soc*. **2004**, *151*, R360.

(26) (a) Mesaric, S. S.; Hume, D. N. *Inorg. Chem*. **1963**, *2*, 1063. (b) Cotton, F. A.; Willkinson, G.; Murillo, C. A.; Bochman, M. *Advanced Inorganic Chemistry*, 6th ed.; John Wiley & Sons: New York, 1999; pp 868 and 1084.

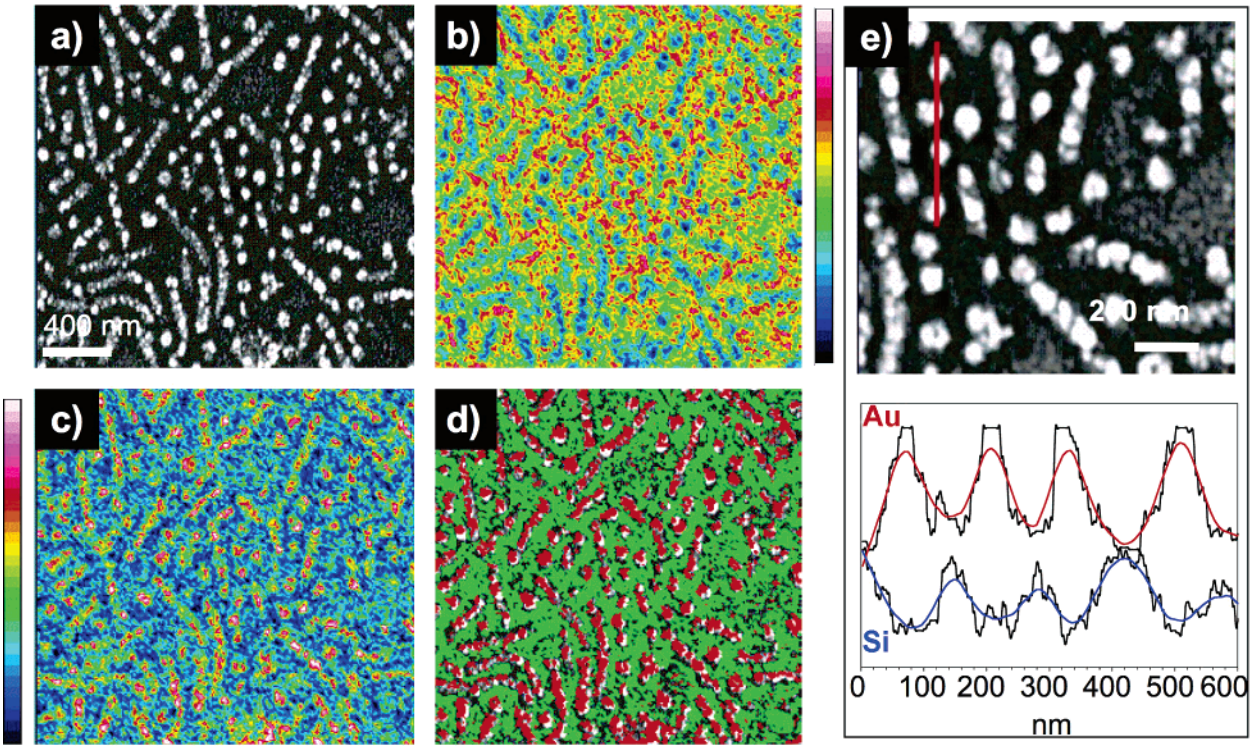

Figure 5. Scanning Auger microscopy (SAM) images of Au nanostructures on SiO_x. (a) SEM image, (b) Si KLL SAM, (c) Au MNN SAM, (d) fitting Au MNN (red) and Si KLL (green) intensities over (a), and (e) SAM line profiles of (top) Au MNN and (bottom) Si KLL. The line positions are shown in red in the SEM image. The depositions were carried out from 0.1 mM $HAuCl_4$/0.9% HF(aq) for 10 min.

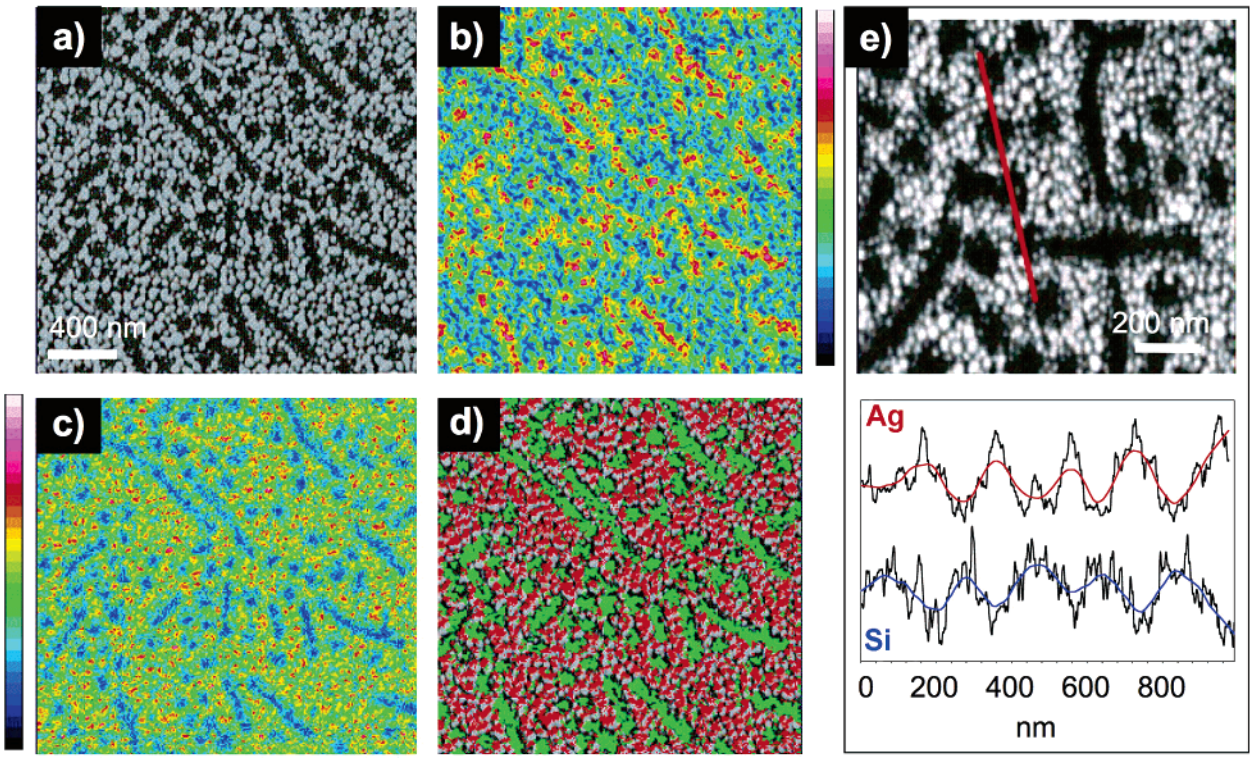

Figure 6. SAM of Ag nanostructures on SiO_x-capped silicon surfaces. (a) SEM image, (b) Si KLL SAM, (c) Ag MNN SAM, (d) fitting Ag MNN (red) and Si KLL (green) intensities over (a), and (e) SAM line profiles of (top) Ag MNN and (bottom) Si KLL. The line positions are shown in red in the SEM image. The depositions were carried out from 0.1 mM $AgNO_3$/0.9% HF(aq) for 10 min.

conclusions based on SEM images of positive and negative gold and silver galvanic displacement reactions under different polymer blocks.

While SEM and SAM point to metal reduction, only XPS can confirm the spontaneous reduction of the metal ions to M(0) by galvanic displacement. The Au 4f XPS spectra of Figure 7a,b correspond to Figure 3c, showing gold deposited onto the SiO_x wafer in the presence of HF and $HAuCl_4$. The peak position indicates that the majority of Au^{3+} ions are spontaneously reduced to metallic Au on the surface, although the shoulders

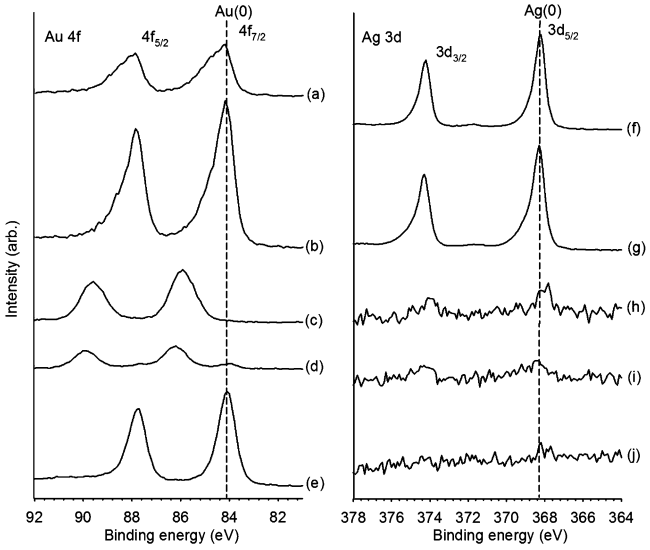

Figure 7. XPS of Au 4f (left) and Ag 3d (right). (a) $HAuCl_4$ deposition on a polymer-coated SiO_x wafer shard in the presence of 0.9% HF(aq). (b) Removal of the polymer via toluene ultrasonication resulted in strengthening of Au signals due to exposure of Au nanoparticles. (c) Same conditions as (a) except reaction carried out in the absence of HF(aq). (d) Polymer removal with toluene ultrasonication led to a decrease of the Au(III) signals. (e) H_2/Ar plasma treatment inducing the reduction of Au(III) and simultaneous polymer removal. (f) $AgNO_3$ deposition on a polymer-coated SiO_x silicon wafer in the presence of 0.9% HF. (g) Removal of the polymer with toluene ultrasonication has no effect on the Ag intensity since Ag nanoparticles are deposited underneath a thin PEO film. (h) Same conditions as (f) except the reaction carried out in the absence of HF. (i) Sample from (h) after polymer removal with toluene ultrasonication. (j) Sample from (h) after H_2/Ar plasma treatment.

on the main peak at higher binding energy suggest a small fraction of species with oxidation states higher than 0.[12] Polymer removal intensified the Au signal due to the exposure of the nanoparticles (Figure 7b). To ensure that metal reduction and deposition is not mediated by PEO oxidation,[16,27,28] the same reaction was carried out in the absence of hydrofluoric acid, the essential ingredient that exposes the underlying silicon through SiO_x dissolution. As shown in Figure 7c, all observable gold is present exclusively as Au(III),[6q,r] and thus no polymer-induced reduction occurs under these conditions. Toluene ultrasonication largely removes most of the Au(III) ions (Figure 7d) as the polymer dissolves in the solvent, taking the bound gold ions with it. In contrast to H_2/Ar plasma, reduction of the Au(III)-loaded polymer from Figure 7c leads to gold metal deposition, as would be expected (Figure 7e) on the basis of earlier results with P2VP-containing block copolymers.[7,11]

Similar XPS results were obtained for silver deposition as well (Figure 7f−j), although several significant differences were noted; the XPS spectra correspond to the samples imaged in Figure 4a,b. First, polymer removal (Figure 7f,g) following silver galvanic displacement did not result in an obvious increase in intensity of XPS signals due to the fact that the PEO block is thin and does not coat the deposited silver metal uniformly. Second, immersion of the polymer-coated SiO_x wafer into aqueous $AgNO_3$ in the absence of HF(aq) shows low levels of silver, certainly due to the thinness of the PEO layer (Figure 7h−j) that prevents significant polymer loading with silver ion. The binding energy difference between Ag^+ and Ag(0) is ~0.4 eV, and therefore the oxidation state of the silver cannot be precisely determined.[29] Since nanoparticles are not observed on the surface by SEM, however, it is doubtful that deposition occurs in the absence of a fluoride source. Like the case with $HAuCl_4$, the block copolymer clearly is not responsible for much or any of the Ag^+ reduction through PEO oxidation. Because silver ions can dissolve in and interact with PEO, it is assumed that transport of silver ions through the thin PEO coating allows for growth of the silver metal nanostructures.[30] The Au(III) salt utilized was either anionic or neutral, and so has less affinity for PEO and does not cross this barrier to the silicon interface.[27]

We assume that the lack of deposition of silver under the P2VP/PS blocks is due to two factors: (i) competition with simple protonation by the HF in the solution (vide supra) for coordination of the silver cation to the pyridine groups, and (ii) the poor coordination ability of the P2VP block as compared to that of a P4VP block. It is expected that the pyridine units in the P2VP shell are predominately protonated under these conditions, and thus the low concentration of silver cations interact little with this block. Even if the silver ion binds to the pyridine, the binding is direct, involving a coordinative Ag−N bond to the sterically hindered 2-pyridine group, whereas the square planar, d^8 Au(III) complex is merely a counteranion of a cationic pyridinium group, and thus is not constrained in this manner. Indeed, Zn(II) salts have been shown to interact to a considerably greater extent with P4VP as opposed to P2VP due to the steric hindrance imposed upon the metal cation when binding directly to a 2-pyridine group.[31] These two factors together can explain the observed spatial directing ability of this block copolymer monolayer.

Since the gold and silver deposit in different blocks of the PS-*b*-P2VP-*b*-PEO polymer, it is therefore possible to generate metallic patterns that consist of a gold center, surrounded by silver shell, via sequential dipping of the polymer-coated silicon wafer in aqueous metal ion solutions. The order in which the dipping is carried out is critical due to the different oxidation/reduction potentials of the metals and metal ions. Because Au(III) has a higher oxidation potential compared with Ag(0), gold was intentionally deposited first. The triblock copolymer-coated silicon wafer was immersed into the 0.1 mM $HAuCl_4$/0.9% HF(aq) solution for 1 min, followed by rinsing with water. The sample was then immersed into 0.1 mM $AgNO_3$/0.9% HF(aq) for 1 min. Figure 8a,b shows SEM images of Au/Ag nanostructures after removal of the polymer with toluene ultrasonication. The Au nanoparticles ~5 nm in diameter are surrounded by larger Ag nanoparticles >10 nm in diameter, forming the Au core and Ag shell nanostructured films. Figure 8c,d shows SEM images of the Au/Ag nanostructures obtained by the same deposition procedure described above, but the Au and Ag deposition times were increased to 5 and 20 min, respectively. Under these conditions, there is increased gold deposition (sufficient for visualization by SAM), and Ag nanoparticles nucleate and grow selectively at the boundary regions between the P2VP and PEO. Silver nanoparticle nucleation on the silicon

(27) (a) Sakai, T.; Alexandridis, P. *Langmuir* **2005**, *21*, 8019. (b) Sakai, T.; Alexandridis, P. *Langmuir* **2004**, *20*, 8426.
(28) Liz-Marzan, L.; Lado-Tourino, I. *Langmuir* **1996**, *12*, 3585.
(29) Wagner, C. D.; Naumkin, A. V.; Kraut-Vass, A.; Allison, J. W.; Powell, C. J.; Rumble, J. R., Jr. *NIST X-ray Photoelectron Spectroscopy Database*, Version 3.4 (Web Version), 2003.
(30) (a) Rao, S. S.; Rao, K. V. S.; Shareefuddin, M.; Rao, U. V. S.; Chandra, S. *Solid State Ionics* **1994**, *67*, 331. (b) Sunderrajan, S.; Freeman, B. D.; Hall, C. K.; Pinnau, I. *J. Membr. Sci.* **2001**, *182*, 1. (c) Liu, L.; Feng, X. S.; Chakma, A. *Sep. Purif. Technol.* **2004**, *38*, 255.
(31) Kuo, S.-W.; Wu, C.-H.; Chang, F.-C. *Macromolecules* **2004**, *37*, 192.

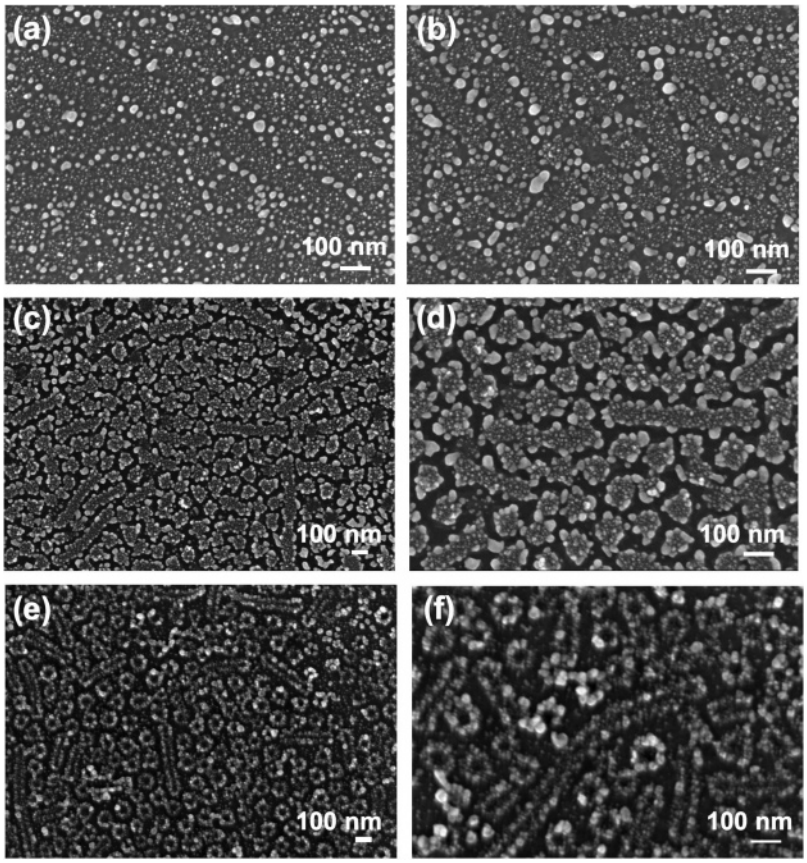

Figure 8. SEM images of AuAg nanostructures on SiO_x-capped silicon wafer shards. The Au and Ag galvanic displacement depositions were carried out in 0.1 mM $HAuCl_4$/0.9% HF(aq) and 0.1 mM $AgNO_3$/0.9% HF(aq), respectively. (a) Au deposition (1 min) followed by Ag (5 min), (b) Au (1 min) followed by Ag (10 min), (c,d) Au (5 min) followed by Ag (20 min), and (e,f) Ag (5 min) followed by Au (10 min) deposition.

most likely becomes disfavored when more gold is deposited due to cathodic protection, and so it occurs preferentially at defect sites on or near the Au/Si interface, or on the gold surface itself.[23i,32] At the edge of sensitivity limits for SAM, it is clear that silver deposition takes place around the micelle core and not within, while for gold it is the opposite (Supporting Information). XPS of these interfaces indicate that, as the Ag deposition time increases, both the Au 4f and Ag 3d X-ray photoelectron spectra shift toward lower binding energy (Supporting Information). The broad Au 4f XPS feature becomes narrower and keeps shifting toward lower binding energy as the Ag deposition proceeds. This is likely due to partial electron transfer from Ag to Au nanoparticles at the boundaries; such intermetallic electron transfer has been reported for AuAg alloys.[33] The resulting $Ag^{\delta+}$ can react with OH^- or O_2 in solution to form Ag_2O or AgO.[34] These oxide peaks are known to shift toward lower binding energies by 0.1−0.9 eV compared to the metallic peak.[29] When the order is reversed and silver is deposited first, the Au(III) ions first undergo a galvanic displacement reaction with the silver metal, dissolving the silver structures. Simultaneously, gold deposition takes place on the silicon but only at the interface between the PEO and P2VP blocks, leading to ring structures of gold (Figure 8e,f). SAM reveals very weak Ag MNN signals and an intense Au pattern (Supporting Information). The reason for the ring structure formation is cathodic protection of the silicon: the electronegativity of the metal deposits (silver initially, followed by subsequent gold growth) ensures that electron flow occurs exclusively via the existing metal on the surface, preventing nucleation in surrounding areas.[23i,32] Just as importantly, the $AuCl_4^-$ anion is selectively transported through the protonated P2VP block, and so growth is limited to the interface between the P2VP and PEO blocks since $AuCl_4^-$ cannot pass through the PEO-covered surface.

Conclusions

The chemical selectivity of block copolymers can be utilized to direct spatially defined surface chemistry on semiconductors. In this case, an ABC triblock copolymer, PS-*b*-P2VP-*b*-PEO, can act as a self-assembled template to deposit metallic nanostructured films on silicon surfaces by an aqueous galvanic displacement reaction. The P2VP and PEO blocks discriminate between anionic compounds and water-solvated cations, leading to positive and negative patterning, with respect to the block copolymer micelle cores. The silver and gold ions interact with the P2VP and PEO blocks in different manners, resulting in the observed selectivity of deposition: the reaction of silicon and Au(III) occurs only in the region of the P2VP block, and silicon and silver(I) react only in the PEO corona. Through sequential dipping procedures, it is possible to form metallic core/shell films of gold and silver, if gold is deposited first. If silver is deposited initially, only gold rings form due to a galvanic displacement between Au(III) and Ag(0), due to the higher oxidizing ability of gold with respect to silver. To

(32) Aizawa, M.; Cooper, A. M.; Malac, M.; Buriak, J. M. *Nano Lett.* **2005**, *5*, 815.
(33) Yamamoto, M.; Nakamoto, M. *Chem. Lett.* **2004**, *33*, 1340.
(34) Qian, L.; Yang, X. *Colloids Surf. A* **2005**, *260*, 79.

summarize, the chemical selectivity of ABC triblock copolymers can be harnessed to direct the reaction of reagents to the surface in a spatially defined manner. This work is presently being extended toward the chemical selectivity of aligned triblock copolymer structures for both metal and organic deposition chemistry on semiconductor interfaces.

Acknowledgment. We thank the National Research Council (NRC) of Canada, the University of Alberta, NSERC, and the Canadian Foundation for Innovation (CRC to J.M.B.). Dr. Dimitre Karpuzov and his colleagues at the Alberta Centre for Surface Engineering and Science (ACSES) are thanked for their considerable assistance with scanning Auger microscopy (SAM), XPS, and other surface science techniques.

Supporting Information Available: SEM images referred to in the text, higher resolution SAM images, AFM images, and XPS spectra. This material is available free of charge via the Internet at http://pubs.acs.org.

JA060366X